

Mach-Zehnder lattice based tunable chromatic dispersion compensator design with simplified control and dispersion slope mitigation

Reinhold Noé

Univ. Paderborn, Optical Communication and High-Frequency Engineering, Warburger Str. 100, D-33098
Paderborn, Germany
noe@upb.de

Zhan Gao

Infineon Technologies AG, Otto-Hahn-Ring 6, 81739 München, Germany

Abstract: The number of externally controlled phase shifts is halved if the power equidistribution between the branches is monitored and controlled in each Mach-Zehnder section. Suitably chosen delays yield an increased tunability and, in multichannel compensators, a selectable dispersion slope.

Keywords: chromatic dispersion compensator, dispersion slope, differential group delay profile

Introduction

Planar lightwave circuits are attractive for the realization of tunable chromatic dispersion compensators because an integration with wavelength DEMUXs is possible. Starting with pioneering work [1] a number of practical equalizers have been reported, e.g. [2-5]. Each stage has a coupler which is adjusted according to the required chromatic dispersion. However, the differential phase shift in each of the differential group delay (DGD) sections also needs to be adjusted. It is difficult to keep track of that, at least if the substrate temperature floats. This limits the practically controllable number of Mach-Zehnder stages. Other issues of interest are a wide tunability range, and dispersion slope mitigation. Dispersion slope compensation has been shown [3, 4], but only on an intrachannel basis, not in such a way that the chromatic dispersion varies from channel to channel. Improvements in several areas of compensator design are proposed here: Local control of the differential phase shifts using monitor diode taps, nonnegligible DGDs in tunable couplers for dispersion slope mitigation in WDM multichannel devices, and apodization of DGDs vs. position for optimized tunability.

Compensator structure and power splitting control

Consider the schematically sketched planar waveguide structure of Fig. 1. There are n sections DGD_i ($i=1\dots n$) with DGDs t_i , separated by $n-1$ tunable couplers C_i . Each DGD section is directly followed by a differential microheater (hatched) which introduces a differential phase shift j_i . The input light is being split in a coupler C_{in} with equal powers into both branches of DGD_1 . After the last DGD section DGD_n an output coupler C_{out} directs most of the light into one output waveguide. Each tunable coupler C_i consists of two cascaded 3dB couplers, separated by an auxiliary DGD section with a DGD $t_{C,i}$ and an auxiliary differential phase shift $j_{C,i}$. We assume all wt_i , $wt_{C,i}$ are odd multiples of π at the carrier frequency w of a channel in the middle of a WDM band. The various $j_{C,i}$ are controlled externally to adjust the chromatic dispersion. All j_i need to be adjusted in such a way that the powers in both waveguides after passing C_{i+1} are equal. This is possible if we place two taps at the outputs of the next coupler C_{i+1} . The difference of the detected tap signals is integrated, and the integrator output controls j_i . This local feedback greatly eases the control requirements because it halves the number of external control variables. If a true 3dB input coupler C_{in} can not be fabricated reliably it can be made variable by a differential phase shift j_{in} between two nominal 3dB couplers, the phase shift being controlled to yield equal power distribution in DGD_1 . An analogous procedure can be implemented to control light focusing into the output waveguide. For this the output coupler C_{out} must have three outputs. The signal exits at the center

waveguide, and the light power difference between the two lateral monitor outputs is made to become zero by suitable adjustment of the last differential phase shift \mathbf{j}_n .

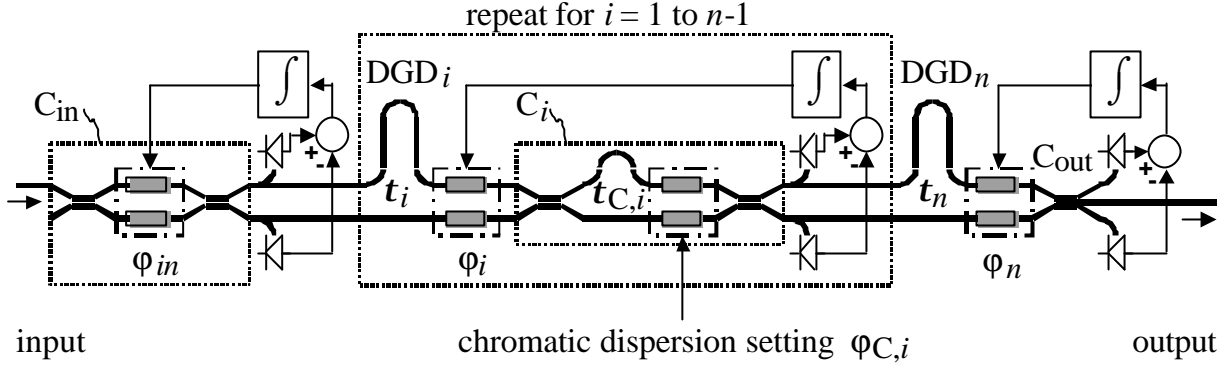


Fig. 1: Schematic of planar chromatic dispersion compensator

Compensator structure and power splitting control

Lossless coupling and differential delay of two modes can be represented in the normalized Stokes space by so-called DGD profiles, as has been explained for the case of polarization mode dispersion in [6]. The DGD or PMD vector was defined here to point in the direction of the fast mode and to have a length which equals the DGD. In the tunable dispersion compensator the modes are not two orthogonal polarization modes but two equipolarized modes in either arm of the lattice structure. The DGD profile is a sequence of concatenated DGD or PMD vectors in a common, input-referred reference system. Therefore each of them is backtransformed by the transposes of all 3×3 rotation matrices which represent in the normalized Stokes space the 2×2 complex transfer matrices of the two electric field modes. In doing so, all couplers and all DGD sections prior to the element under consideration have to be taken into account in the correct order.

To give an example, we consider $n=12$, $\mathbf{t}_{1,11}=-\mathbf{t}_{2,12}=5\text{ps}$, $\mathbf{t}_{3,5,7,9}=-\mathbf{t}_{4,6,8,10}=10\text{ps}$, $\mathbf{j}_{1\dots 12}=0$, $\tau_{C,1\dots 11}=-25\text{fs}$, $\mathbf{j}_{C,i}=0$. This choice allows for a fairly regular, space-saving meandering waveguide pattern. At the center frequency the DGD profile is depicted in Fig. 2. The input signal which is fed to one interferometer arm is represented by an input arrow in Ω_1 direction. The various rods in the Ω_2 - Ω_3 plane represent DGD_i and have lengths t_i . They must lie in the Ω_2 - Ω_3 plane. This corresponds to equal power splitting between the two arms, which is achieved by the local control loops. Otherwise the dispersion compensation capability could be seriously hampered. Between the DGD_i there are rods along Ω_1 with lengths $t_{C,i}$, representing the DGD sections inside coupler C_i . Note that the Ω_1 coordinate in Fig. 2 is stretched by a factor of 50 for better viewability. Each rod twists about its own axis as a function of \mathbf{w} because its differential phase shift $\mathbf{w}t_i$, $\mathbf{w}t_{C,i}$ is proportional to \mathbf{w} . The angle change between various rods represents mode coupling. The 3dB couplers C_{in} , C_{out} as well as those inside C_i are represented by concentrated 90° turns. Looking at the whole DGD profile, if θ is the angle between the output arrow and the input arrow (along Ω_1) then $\cos^2\theta$ is the power fraction transmitted to the output. According to the above DGD vector definition the group delay experienced by the signal is $-1/2$ times the Ω_1 coordinate of the DGD profile endpoint. The factor $1/2$ applies because the DGD equals the difference of the group delays of one mode, which is exited, and the other mode, which could be exited at the other, unused input port of C_{in} . A *linear movement of this endpoint as a function of \mathbf{w}* is necessary for chromatic dispersion compensation.

A simulated 43Gbit/s eye diagram is shown in Fig. 3 left. It virtually coincides with the back-to-back eye diagram. In the vicinity of the center frequency the DGD profile stays very similar to that of Fig. 2 because the frequency-dependent twists of adjacent but oppositely directed sections DGD_i cancel well.

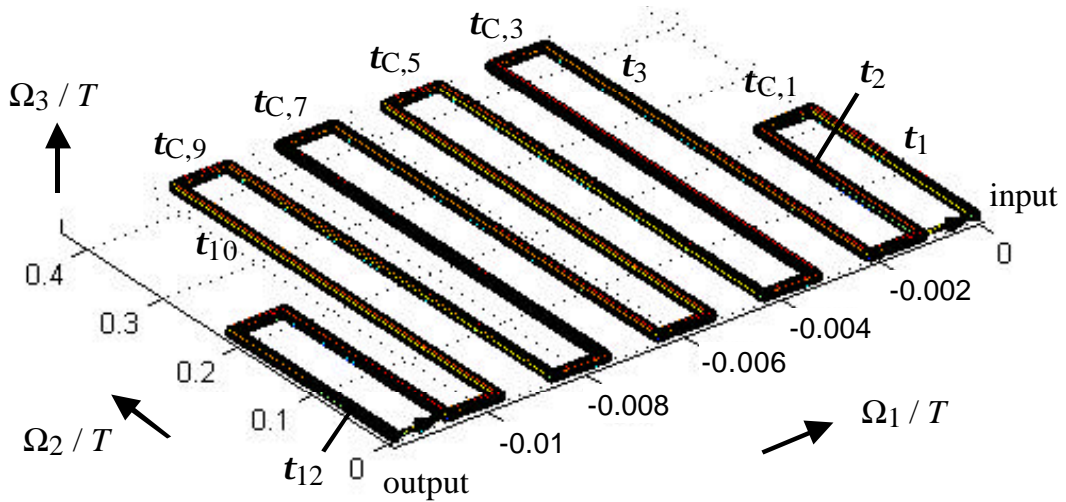


Fig. 2: DGD profile without chromatic dispersion at the center frequency. Scaling unit is the bit duration $T = 23.3\text{ps}$.

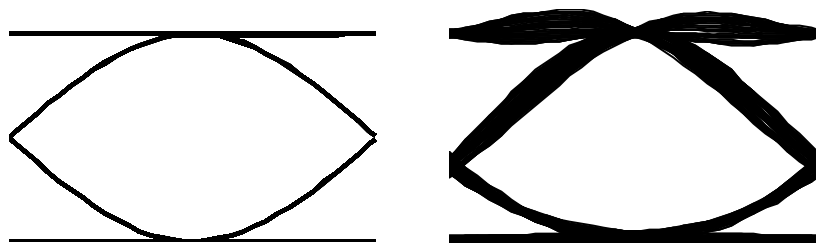


Fig. 3: Simulated 43Gbit/s eye patterns behind compensator, with 0ps/nm (left) or 160ps/nm (right) of chromatic dispersion compensated

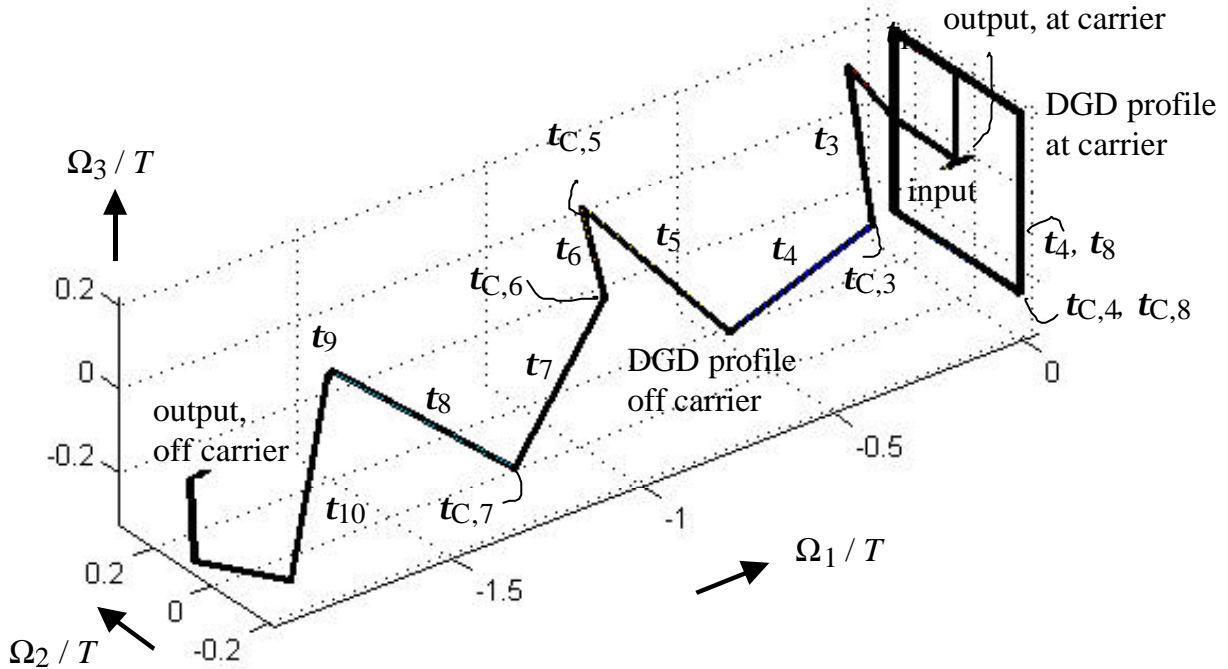


Fig. 4: DGD profile at carrier frequency and 20GHz off carrier when a 160ps/nm chromatic dispersion is compensated, using $j_{c,i} = -\pi/2$. – When $j_{c,i} = 0$ is used, Fig. 2 applies for a centered carrier frequency, and Fig. 4 simultaneously applies for a carrier frequency having a -10THz offset with respect to the centered carrier frequency. A $\sim 2\text{ps/nm}^2$ dispersion slope compensation is thereby provided.

Next we want to compensate for the chromatic dispersion DL (given in ps/nm) of a transmission fiber. A fairly good coupler phase shift setting is $\mathbf{j}_{C,i}=0.0098*DL$, valid up to about $|\mathbf{j}_{C,i}|=0.6\pi$. This corresponds to a $\sim\pm 190$ ps/nm tuning range. Individual optimization of the $\mathbf{j}_{C,i}$ yields a slightly wider tuning range. For $\mathbf{j}_{C,i}=-\pi/2$ the DGD profile at the center frequency looks like a “discrete” spiral (right part of Fig. 4). All DGD_{*i*} rods lie essentially in one plane. 20 GHz higher the DGD profile spiral is pushed far apart by the twist of the rods about their axes, thereby providing the desired wavelength dependence of the group delay (rest of Fig. 4). For negative frequency offsets the spiral extends in the other direction. Obviously, a symmetry of \mathbf{t}_i and $\mathbf{j}_{C,i}$ settings with respect to the center of the compensator yields a regular DGD profile and is advantageous. Fig. 3 right shows the eye diagram if a 160ps/nm fiber dispersion is now compensated.

The DGD profile repeats every 200ps, but not exactly because of the non-zero $\tau_{C,i}$. With $\mathbf{j}_{C,i}=0$ the DGD profile at the center frequency is given by Fig. 2. A large frequency offset lets the DGD sections inside C_i twist noticeably. Specifically, for a carrier frequency offset of -10THz, where they twist by 1/4 turn, and for a frequency offset of -9.98THz the DGD profiles are again given by Fig. 4, and the eye diagram while compensating 160ps/nm is given by Fig. 3 right. This shows that the device compensates a dispersion slope of ~ 2 ps/nm². The slope compensation changes its sign if we set $\mathbf{j}_1=\mathbf{j}_{12}=\pi$ and replace the signs of all $\mathbf{j}_{C,1\dots 11}$. This has the same effect as a sign change of all $\tau_{C,1\dots 11}$. The desired dispersion slope must be chosen when compensation starts. Later it can not be changed online without temporary loss of compensation. Compensation of much larger (e.g., 10ps/nm²) or smaller slopes can also be implemented by proportional changes of the $\tau_{C,i}$. More finely selectable or truly variable amounts of slope compensation require more complicated variable coupler structures. These can be found intuitively using DGD profiles.

Another feature of our design example is the apodization of the \mathbf{t}_i vs. i . Here the two first and two last DGD sections are shorter than the middle ones, more than in [1]. The apodization greatly reduces unwanted distortions, in our case at the expense of the need for two separate compensators and AWG DEMUXs for even and odd 100GHz-spaced WDM channels. The quantized \mathbf{t}_i yield periodic dispersion compensation windows. If periodicity is not needed then a \mathbf{t}_i apodization similar to a single sine halfwave (sampled from 0 to π for $i = 1$ to n) may be more advantageous.

Summary

Solutions to several design issues of Mach-Zehnder lattice based tunable dispersion compensators have been proposed: Local control of the differential phase shifts using monitor diode taps halves the number of degrees-of-freedom. Nonnegligible DGDs in the tunable couplers provide a dispersion slope with selectable sign for WDM multichannel operation. Apodized DGDs vs. section number optimize the tunability. Not the least, the representation by DGD profiles provides a graphical understanding of Mach-Zehnder lattices and allows an intuitive design of these and other advanced structures.

- [1] M. Sharma et al., *J. Lightwave Technology*. **JLT-12**, 1759-1765, 1994
- [2] K. Takiguchi et al., *J. Lightwave Technology*. **JLT-14**, 2003-2011, 1996
- [3] K. Takiguchi et al., *J. Lightwave Technology*. **JLT-16**, 1647-1656, 1998
- [4] G.L. Bona et al., *Proc. ECOC2002*. Copenhagen, Denmark, Vol. II., 4.2.1, 2002
- [5] M. Bohn et al., *Proc. ECOC2002*. Copenhagen, Denmark, Vol. II., 4.2.3, 2002
- [6] R. Noé, *Proc. ECOC2002*. Copenhagen, Denmark, Vol. II., T4, 2002